Estimation of X-band radar attenuation due to wet hail: A simulation study using RAMS supercell case and dual-wavelength (S/X-band) radar

Y.X. Liu, G.J. Huang, V.N. Bringi and S. van den Heever
Colorado State University, Fort Collins, CO 80523-1373, USA

1 Introduction

The recent resurgence of dual-polarization X-band weather radar is largely due to the accurate correction for rain attenuation which is made possible using the measurement of differential propagation phase (Φ_{dp}) between H and V polarizations. A number of different algorithms are now available for rain attenuation-correction using Φ_{dp} (either directly or as a constraint; e.g., Bringi et al 1990; Matrosov et al 2002; Testud et al 2000; Gorgucci et al 1996; Park et al 2005).

When rain is mixed with wet ice which is a frequent occurrence in convective storms, the Φ_{dp}-based method will be in error because wet ice (snow/graupel/hail) contributes very little to the Φ_{dp} (being nearly isotropic) whereas it does contribute significantly to the radar reflectivity. While the attenuation due to the rain component of the mixture can be calculated using Φ_{dp}, the attenuation due to wet ice component is very difficult to estimate because of the large variability in the size distribution and water coat thickness which gives rise to large family of k-Z relations (k is the specific attenuation, Z is the intrinsic reflectivity). In the past, the dual-wavelength (S/X-band) radar technique was developed primarily for hail detection (sizes > 10 mm) but did need attenuation-correction of the X-band signal due to rain and wet ice along the path (e.g., Tuttle and Rinehart 1983). Tuttle et al (1989) showed the vertical structure of the total (rain+wet ice) specific attenuation field at X-band in a microburst-producing storm.

In this paper we report on a technique to separately estimate the X-band specific attenuation due to rain and wet ice along the path assuming that a dual-wavelength radar (S/X bands; dual-polarized at S-band) is available (such as the NCAR CP2 radar; Bringi and Hendry 1990). Note that the CP2 radar is due to be installed near Brisbane, Australia this year and operated by the Bureau of Meteorology (BoM; Keenan, personal communication). The technique is developed and evaluated using the microphysics outputs from a RAMS supercell simulation described in van den Heever and Cotton (2004); see, also the corresponding S-band radar simulations reported in Huang et al (2005).

Correspondence to: Y.X. Liu
liuyx@engr.colostate.edu

2 Background

We assume that we have available the range profile of the dual-wavelength reflectivity ratio ($DWR = Z_h(\mathrm{S})/Z_h(\mathrm{X})$, subscript h denotes H polarization) along with the Φ_{dp} at S-band. The range profile of DWR not only gives the PIA at X-band directly (assuming that the S-band is unattenuated); it can also be used to estimate the specific attenuation at X-band at each range bin using the iterative range filtering method of Hubbert and Bringi (1995) after correcting for any Mie 'hail' signal. This is similar to calculating specific differential phase (K_{dp}) from range profile of Φ_{dp} after correcting for the Mie backscatter differential phase.

When the propagation path traverses the mixed phase region (rain+wet hail), the $K_{dp}(\mathrm{S})$ and the $PI\Phi_{dp}$ (path integrated Φ_{dp}) are only due to oriented, oblate raindrops along the path and independent of the approximately isotropic wet ice particles along the path (see Chapter 4 of Bringi and Chandrasekar 2001). In addition, there is good theoretical and observational evidence that differential propagation phase and rain attenuation are highly correlated and one is derivable from the other (Bringi and Chandrasekar 2001). Thus, we can estimate the rain component of the X-band attenuation from the Φ_{dp} data at S-band. On the other hand, the total specific attenuation and the PIA at X-band are due to both rain and wet ice along the path (the contributions of cloud water and gaseous attenuation are neglected here which is reasonable at X-band). By simply differencing the total (= rain+wet ice) measured attenuation at X-band from the estimated rain attenuation, we can estimate the attenuation due to wet ice separately from the rain portion. This will also enable determination of the vertical extent of the rain and wet ice

specific attenuation fields separately, as well as the vertical extent of the total attenuation field. The anticipated application of dual-polarized X-band radar networks for hydrology or as 'gap fillers' for regions that cannot be covered by S or C-band radar networks implies that attenuation-correction by wet ice needs further study (Chandrasekar et al 2004).

3 Simulation Results

Fig. 1 shows a vertical section of contours of specific attenuation at H polarization (A_h) of rain and hail at X-band (9.3 GHz here) using the RAMS output of mixing ratios of hail and rain at each grid point. The simulations assume that hail is wet when occurring below 6 km in height (see Huang et al 2005 for details). Note the overlap between the hail and rain regions which we refer to as the mixed phase region. The background is the input or 'true' X-band Z_h intensity plot.

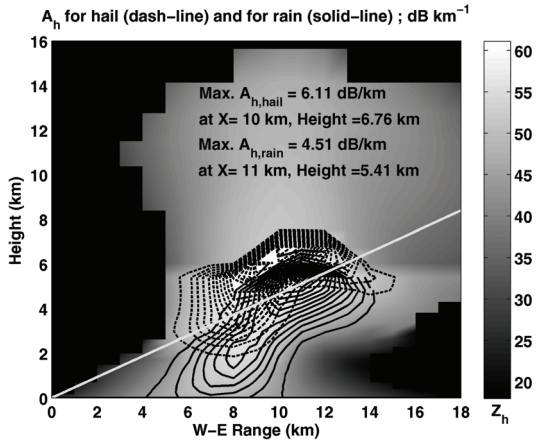

Fig. 1. Vertical section of contours of specific attenuation (A_h) of rain and hail at X-band. Dash line is hail A_h contour. Solid line is rain A_h contour. The 'true' X-band Z_h is plotted as background.

Fig. 2 shows the range profile of the *DWR* (or, *PIA*) along the slant path (plotted as a slant solid line in Fig. 1) at 25° elevation angle with the radar located at the bottom left corner in Fig. 1 (both the 'true' values from the RAMS-based scattering calculations as well as the profile with added Gaussian noise of σ=0.75 dB to the S and X band signals are shown). The *PIA* is due to both rain and wet hail along the path and at the end of the path the total *PIA* is around 54 dB. As shown by Tuttle and Rinehart (1983) using CP-2 data, such total *PIA* is common in supercell hailstorms (though their goal was to derive the Mie 'hail' signal after correcting the measured X-band Z_h for path attenuation).

Fig. 2 also shows the *PIA* due to rain attenuation only along the same path by converting the 'measured' S-band K_{dp} to X-band rain attenuation. The S-band K_{dp} is estimated from the Φ_{dp} with added Gaussian noise (σ=2°) for realism. Also, the relation between S-band K_{dp} and X-band A_h is calculated based on theoretical rain DSD simulations ($A_h(X)=0.95*K_{dp}(S)$). Fig. 2 shows that the rain *PIA* can be estimated to within a few dB of its 'true' value (27 dB).

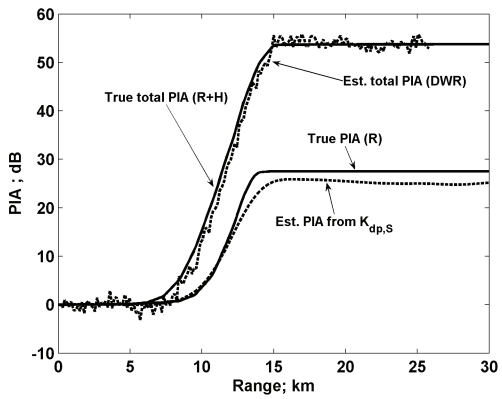

Fig. 2. Range profiles of the *DWR* along the slant path at 25° elevation angle, 'true' total PIA, 'true' rain PIA, and estimated rain PIA.

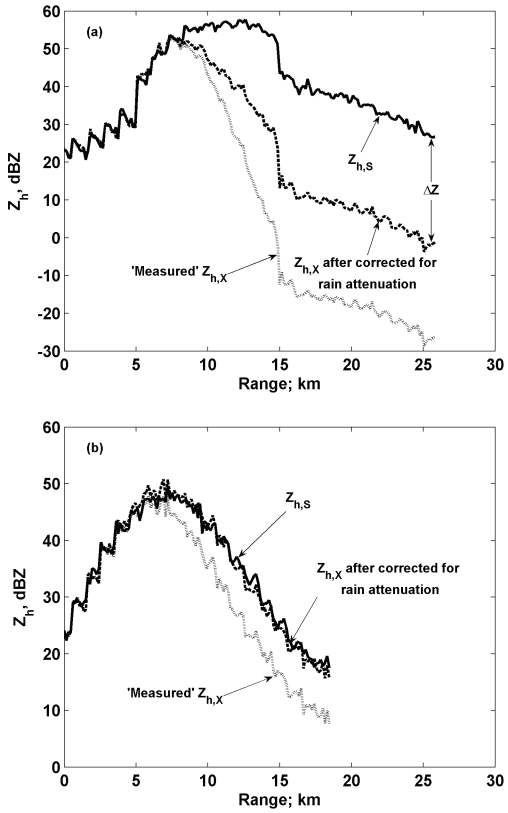

Fig. 3. Range profiles of Z_h(S), the attenuated (or 'measured') Z_h(X), and Z_h(X) corrected for rain attenuation only. (a) at 25° elevation angle, (b) at 0.5° elevation angle.

Fig. 3 shows the range profile of S-band reflectivity, the attenuated X-band reflectivity (due to rain+wet hail) and the X-band reflectivity corrected for rain attenuation only using the S-band Φ_{dp}. Fig. 3a shows the profile at 25° elevation angle (same as in Fig. 2). This figure clearly shows the range of error that can occur due to excess attenuation of wet hail which cannot be accounted for by the Φ_{dp}. In contrast, Fig. 3b shows the similar profiles at low elevation angle (0.5°) where hail is essentially absent. Note that the attenuation-correction is, as expected, quite accurate (the ZPHI method of Testud et al 2000 gave similar results and not shown here).

4 Retrieval of specific attenuation fields at X-band

The specific attenuation field due to rain can be obtained from the K_{dp} (a number of filtering methods are available for estimating K_{dp} from the Φ_{dp}; e.g., Bringi and Chandrasekar 2001, see chapter 6). In similar manner, the total specific attenuation (due to rain+wet hail) can be obtained from the range profile of the *DWR* as A_{h_total}=0.5*dDWR*/*dr*. The assumption is that the 'true' or intrinsic $Z_h(S)$-$Z_h(X)$ is uniform within Δr. Note that if Mie hail signal exists along a section of the path (true $Z_h(S)$-true $Z_h(X)$ > 3 dB), it can be 'suppressed' by the iterative filtering method of Hubbert and Bringi (1995) similar to 'suppression' of the back scatter differential phase in the K_{dp} estimation procedure. In the RAMS simulations the mean mass diameter of the hail was set to 3 mm which generally excluded Mie hail signals. van den Heever and Cotton (2004) also simulated a supercell case with hail mean mass diameter of 1 cm for which such Mie hail signals do occur over a significant region of the simulated storm.

The specific attenuation field due to wet hail can be separated from the total attenuation by subtracting the rain attenuation from the total attenuation field. Fig. 4 shows contours of specific attenuation of the wet hail in the vertical plane, (a) the input or 'true' values from the RAMS microphysical output (see also Fig. 1), and (b) the retrieved values. Note the close correspondence in the vertical structure of the contours. Because of smoothing the *DWR* profile, the peak of the retrieved values will be lower than the 'input' peak as expected; however, the values are within around 0.5 dB/km which is the expected error of the retrieval.

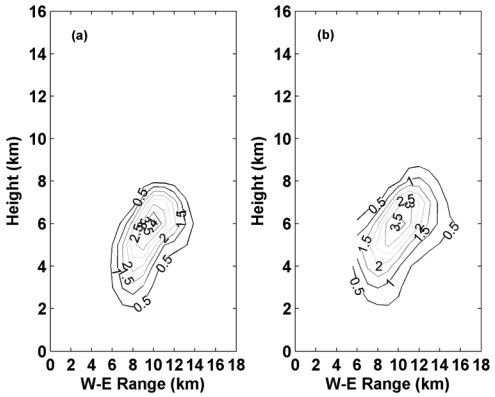

Fig. 4. Contours of specific attenuation of the wet hail in the vertical section. (a) the 'true' values from the RAMS microphysical output, (b) the retrieved values.

Fig. 5 shows similar comparisons between the rain specific attenuation fields with (a) the input or 'true' values from the RAMS microphysics output, and (b) the retrieved values. In agreement with prior work, the rain specific attenuation field can be accurately retrieved within the constraints of smoothing the Φ_{dp} profile to get K_{dp}. Since smoothing the Φ_{dp} profile is not necessary in the ZPHI method, it is preferred if the propagation path is in rain only (peak values are better retrieved).

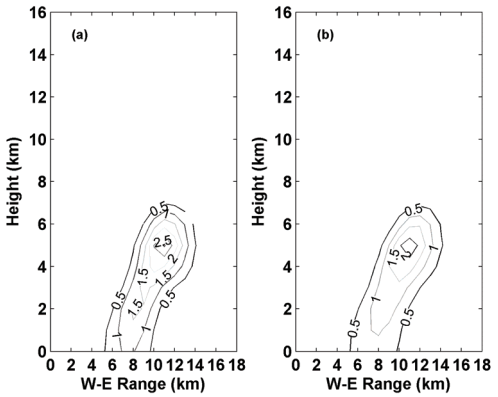

Fig. 5. Contours of specific attenuation of rain in the vertical section. (a) the 'true' values from the RAMS microphysical output, (b) the retrieved values.

5 Extension to single wavelength with external constraint

With a single wavelength (X-band) dual-polarized radar it is difficult to correct for wet ice attenuation without some sort of external constraint since *k*-*Z* relations can be highly variable and Φ_{dp}, in general, gives no additional information in wet ice. One possibility, at least within the U.S. is to use the S-band WSR-88D to give an external *DWR*-like constraint at the end point of the X-band radar beam (i.e., a pseudo dual-wavelength scheme with separated radars rather than a matched beam system such as the CP2 radar). To illustrate, Fig. 3a shows the ΔZ as a *PIA* constraint (about 28 dB) at the end of the beam (after $Z_h(X)$ has been corrected for rain attenuation). One technique is the TRMM SRT α-adjustment method (Iguchi et al 2000) that can be used to apportion the ΔZ or *PIA* backwards along the beam assuming a $k=\alpha Z^{\beta}$ relationship with fixed β. The α is adjusted such that the total calculated *PIA* will match the ΔZ at the end of the beam. The approximation here is that an 'effective' *k*-*Z* relation is suitable for the entire wet ice path. Here, we have used the RAMS wet hail output to estimate the β (0.83, which is larger than the 0.6 value quoted by Tuttle and Rinehart 1983 perhaps because their measurements were made in cases with very large hail whereas the RAMS simulations used here assume mean mass diameter of 3 mm for the hail species).

Fig 6. shows the profile of $Z_h(X)$ after correction for both rain and wet hail as compared with the input or 'true' $Z_h(X)$ profile. The agreement is good and within a few dB over the entire beam. However, we do not expect such performance with spatially separated X and S band radars. The practical considerations and potential errors are a topic of future study.

It is also possible to retrieve the wet hail specific attenuation field using this TRMM SRT-like method. The wet hail specific attenuation can be calculated using the adjusted *k*-*Z* relation. Similar to Fig. 4, Fig. 7 shows contours of wet hail specific attenuation in a vertical plane, (a) the input or 'true' values, (b) the retrieved values. The peak value is better preserved, provided that the *PIA* or ΔZ

can be estimated accurately. Again, we do not expect such performance with spatially separated X and S band radars.

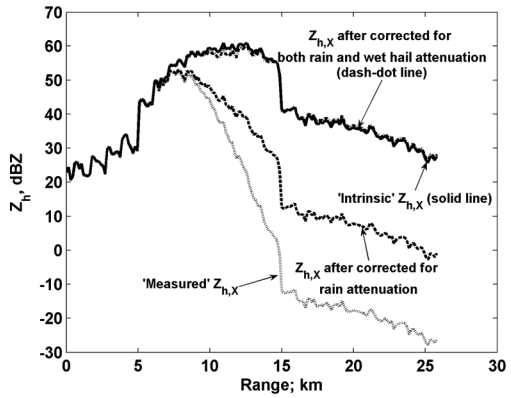

Fig. 6. Profiles of the attenuated (or 'measured') $Z_h(X)$, $Z_h(X)$ after correction for rain only, $Z_h(X)$ after correction for both rain and wet hail, and the 'intrinsic' $Z_h(X)$.

6 Conclusions

We have demonstrated using RAMS supercell simulations that a dual-wavelength (S/X-bands) radar with Φ_{dp} capability at S-band can be used to separately estimate the X-band attenuation due to rain and wet ice along the beam. The methodology extends prior work in the 1970-80s using dual-wavelength radars (such as CP2 or CHILL radars) which did not have Φ_{dp} measurement capability; however, that early work was more focused on hail detection.

Under an NCAR/BoM cooperative agreement the CP2 radar (with Φ_{dp} capability at S-band) will be installed near Brisbane later this year allowing for an experimental evaluation of the techniques proposed and simulated herein. The vertical extent and structure of the separate rain and wet ice specific attenuation fields are expected to be important for convective storm evolution studies as well as providing for validation of the microphysical (rain and hail) parameterizations used in numerical models such as RAMS. When the CP2 measurements become available, it will permit the estimation of *k-Z* relations for wet ice which may improve single wavelength attenuation-corrections schemes (e.g., TRMM radar especially over land).

We also extend the techniques to applications where an external constraint can be obtained, such as a pseudo dual-wavelength radar system. Potential errors may arise in practical conditions. It is a topic of future study to characterize the errors for such applications.

Acknowledgements: This work was supported by the Engineering Research Center program of the NSF under award number 0313747.

References

Bringi, V.N., V. Chandrasekar, N. Balakrishnan, and D.S. Zrnić, 1990: An examination of propagation effects in rainfall on radar measurements at microwave frequencies. *J. Atmos. Oceanic Technol.*, **7**, 829-840.

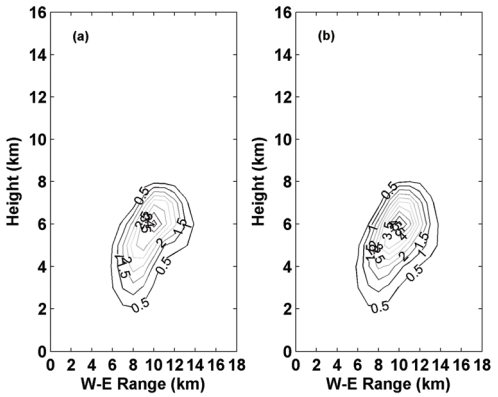

Fig. 7. Contours of specific attenuation of the wet hail in the vertical section. (a) the 'true' values from the RAMS microphysical output, (b) the retrieved values calculated from an adjusted *k-Z* relationship.

Bringi, V.N. and A. Hendry, 1990: Technology of polarization diversity radars for meteorology. In *Radar in Meteorology*. D. Atlas, Ed., 153-190, Boston, MA, American Meteorological Society.

Bringi, V.N. and V. Chandrasekar, 2001: Polarimetric doppler weather radar: principles and applications. Cambridge.

Chandrasekar, V., S. Lim, N. Bharadwaj, W. Li, D. McLaughlin, V.N. Bringi, and E. Gorgucci, 2004: Principles of networked weather radar operation at attenuating frequencies. In *Proceedings*, *ERAD 2004*, 109-114.

Gorgucci, E., G. Scarchilli, and V. Chandrasekar, 1996: Error structure of radar rainfall measurement at C-band frequencies with dual-polarization algorithm for attenuation correction. *J. Geophys. Res.*, **101**, 26461-26471.

Hubbert, J. and V.N. Bringi, 1995: An iterative filtering technique for the analysis of copular differential phase and dual-frequency radar measurements. *J. Atmos. Oceanic Technol.*, **12**, 643-648.

Huang, G.J., V.N. Bringi, S. van den Heever, and W. Cotton, 2005: Polarimetric radar signatures from RAMS microphysics. In *Preprints*, *32nd Conference on Radar Meteorology*, October, 24-29, 2005, Albuquerque,NM. American Meteorological Society.

Iguchi, T., T. Kozu, R. Meneghini, J. Awaka, and K. Okamoto, 2000: Rain-Profiling Algorithm for the TRMM Precipitation Radar. *J. Appl. Meteo.,* **39**, 2038-2052.

Matrosov, S.Y., K.A. Clark, B.E. Martner, and A. Tokay, 2002: X-band polarimetric radar measurements of rainfall. *J. Appl. Meteor.*, **41**, 941-952.

Park, S.G., V.N. Bringi, V. Chandrasekar, M. Maki and K. Iwanami, 2005: Correction of radar reflectivity and differential reflectivity for rain attenuation at X band. Part I: theorectical and empirical basis. *J. Atmos. Oceanic Technol.*, **22**, 1621-1632.

Park, S.G., M. Maki, K. Iwanami, V.N. Bringi and V. Chandrasekar, 2005: Correction of radar reflectivity and differential reflectivity for rain attenuation at X band. Part II: evaluation and application. *J. Atmos. Oceanic Technol.*, **22**, 1633-1655.

Tuttle, J.D. and R.E. Rinehart, 1983: Attenuation correction in dual-wavelength analyses. *J. Climate Appl. Meteor.*, **22**, 1914-1921.

Tuttle, J.D., V.N. Bringi, H.D. Orville, and F.J. Kopp, 1989: Miltiparameter radar study of a micro burst: Comparison with model results. *J. Atmos. Sci.*, **46**, 601-620.

Testud, J., E.L. Bouar, E. Obligis, and M. Ali-Mehenni, 2000: The rain profiling algorithm applied to polarimetric weather radar. *J. Atmos. Oceanic Technol.*, **17**, 322-356.

van den Heever, S.C. and W.R. Cotton, 2004: The impact of hail size on simulated supercell storm, *J. Atmos. Sci.,* **61**, 1596-1609.